Journal of Power Sources 252 (2014) 107–112

Contents lists available at ScienceDirect

Journal of Power Sources

journal homepage: www.elsevier.com/locate/jpowsour

Short communication

# A sulfur–polyacrylonitrile/graphene composite cathode for lithium batteries with excellent cyclability

Jing Li, Kai Li, Mingqi Li, Denise Gosselink, Yongguang Zhang, P. Chen*

*Department of Chemical Engineering, University of Waterloo, Waterloo, ON, Canada N2L 3G1*

## HIGHLIGHTS

- A sulfur–polyacrylonitrile/reduced graphene oxide (SPAN/RGO) composite was prepared.
- The composite consists of RGO decorated by SPAN particles of 100 nm average size.
- It exhibits ~85% retention of the initial reversible capacity of 1467 mAh $g^{-1}$ over 100 cycles.
- It retains 1100 mAh $g^{-1}$ after 200 cycles.
- It displays an 828 mAh $g^{-1}$ reversible capacity at 2C rate.

## ARTICLE INFO

*Article history:*
Received 21 August 2013
Received in revised form
19 November 2013
Accepted 25 November 2013
Available online 7 December 2013

*Keywords:*
Lithium–sulfur batteries
Graphene
Reduced graphene oxide
High capacity
Cyclability

## ABSTRACT

A sulfur–polyacrylonitrile/reduced graphene oxide (SPAN/RGO) composite with unique electrochemical properties is prepared via deposition of PAN on the surface of RGO sheets followed by ball milling with sulfur and heat treatment. Infrared spectroscopy and microscopy studies indicate that the composite consists of RGO decorated by SPAN particles of 100 nm average size. The SPAN/RGO composite shows good overall electrochemical performance when used in Li–S batteries. It exhibits ~85% retention of the initial reversible capacity of 1467 mAh $g^{-1}$ over 100 cycles at a constant current rate of 0.1C and retains 1100 mAh $g^{-1}$ after 200 cycles. In addition, the composite displays excellent Coulombic efficiency and rate capability, delivering up to 828 mAh $g^{-1}$ reversible capacity at 2C. The improved performance stems from the composition and structure of the composite, wherein RGO renders a robust electron transport framework and PAN matrix help suppresses the shuttle effect by absorbing sulfur/polysulfides.



## 1. Introduction

Rechargeable lithium sulfur (Li–S) batteries are safe, environmentally friendly and economical alternative energy storage systems that can potentially be combined with renewable sources including wind, solar and wave energy. Sulfur has a high theoretical specific capacity of ~1680 mAh $g^{-1}$, attainable through the reversible redox reaction denoted as $S_8 + 16Li \leftrightarrow 8Li_2S$, which yields an average cell voltage of ~2.2 V [1]. However, two detrimental factors prevent the achievement of the full potential of the Li–S batteries. First, the poor electrical/ionic conductivity of elemental sulfur and $Li_2S/Li_2S_2$ severely hampers the utilization of active material for obtaining full capacity of the electrode [2]. Second, dissolution of intermediate long-chain polysulfides ($Li_2S_n$, $2 < n < 7$) into the electrolyte and their shuttle between cathode and anode leads to fast capacity degradation and low Coulombic efficiency [3]. As a result of this shuttle process, insoluble and insulating $Li_2S/Li_2S_2$ precipitates on the surface of electrodes causing loss of active material and rendering the electrodes surface electrochemically inactive [4].

Extensive research efforts have been devoted to overcome the aforementioned problems, such as combination of sulfur with conductive polymers [5–9], and encapsulation or coating of elemental sulfur in different nanostructured carbonaceous materials [10–21]. Noteworthy, sulfur–polyacrylonitrile (SPAN) composites, wherein sulfur is chemically bond to the polymer backbone and PAN acts as a conducting matrix, have shown some success in suppressing the shuttle effect [21,22]. However, due to the limited electrical conductivity of polyacrylonitrile, the capacity retention and rate performance of the SPAN systems are still very modest.

Recently, graphene has been intensively investigated for enhancing the rate and cycling performance of lithium sulfur

* Corresponding author.
*E-mail address:* p4chen@uwaterloo.ca (P. Chen).

0378-7753/$ – see front matter © 2013 Elsevier B.V. All rights reserved.
http://dx.doi.org/10.1016/j.jpowsour.2013.11.088

batteries. Graphene, which has a two-dimensional, one-atom-thick nanosheet structure offers extraordinary electronic, thermal and mechanical properties [23–29]. Herein, we report on a sulfur–polyacrylonitrile-reduced graphene oxide (SPAN/RGO) composite prepared by a low-cost and environmentally benign solvent exchange approach. The electrochemical performance of the composite as a cathode material for Li–S batteries was also investigated.

## 2. Experimental section

### 2.1. Materials

Natural graphite (Alfa Aesar), hydrazine (35 wt.% in water), ammonia solution (28 wt. % in water), polyacrylonitrile (average molecular weight 150,000), sulfur, dimethylformamide, sodium chloride, sulfuric acid (concentrated), sodium nitrate, potassium permanganate, hydrogen peroxide (30 wt.%), hydrochloride acid (37 wt.%) (Sigma–Aldrich) were used without further purification, Katjen Black 600 (AkzoNobel), polyvinyldifluoride (Sigma–Aldrich), N-methylpyrrolidone (Sigma–Aldrich). Milli-Q grade water was used in all experiments.

### 2.2. Synthesis procedure

#### 2.2.1. Preparation of reduced graphene oxide (RGO) aqueous suspension

Graphite oxide (GO) was prepared through a modified Hummers method [30]. 0.8 g natural graphite was stirred in 23 ml concentrated $H_2SO_4$ (98%) for 24 h, and 3 g $KMnO_4$ were added to the dispersion while the temperature was kept below 20 °C. The mixture was then diluted and heated up to 100 °C for 15 min. The reaction was terminated by addition of 10 ml $H_2O_2$ solution (30%) and 140 ml water. The resulting graphite oxide was then repeatedly washed with 5% HCl aqueous solution and water. A brown-colored dispersion was achieved. The graphite oxide dispersion was ultrasonicated for 30 min using a Hielscher Ultrasonics (UIP 1000hd, 150W, 50% amplitude).

Next, a reduced graphene oxide (RGO) dispersion was achieved through chemical reduction of GO with the presence of ammonia, which was used to preserve the functional group on reduced graphene oxide to obtain maximal charge density for a stable dispersion of RGO [31]. The GO dispersion was diluted with water to 0.05 wt.%. 100 ml of the homogeneous dispersion was then mixed with 100 ml water, 100 μl hydrazine solution (35 wt.% in water), and 0.7 ml ammonia solution (28 wt.% in water) in a 250 ml round bottom flask. The weight ratio of hydrazine to graphene oxide was 7:10. The flask and its contents were immersed into an oil bath, kept at 95 °C, for 1 h. The excess hydrazine was thoroughly removed by dialysis against 0.5% ammonia solution.

#### 2.2.2. Polyacrylonitrile/reduced graphene oxide composite (PAN/RGO)

100 ml of the as prepared RGO dispersion were mixed with 64 ml of a 5.88 $gL^{-1}$ PAN/DMF solution. After vigorous stirring for 10 min, 600 ml 0.5 wt.% ammonia aqueous solution was added to the beaker and stirred for 24 h. About 0.4 g PAN/RGO sediment was obtained by centrifugation, and repeatedly washing with ethanol and water.

#### 2.2.3. Sulfur–polyacrylonitrile/partially reduced graphene oxide composite (SPAN/RGO)

The PAN/RGO composite obtained by centrifugation was immediately subject to wet ball milling with 1.6 g sulfur at 500 rpm for 3 h. The mixture was then dried in a vacuum oven at 60 °C, followed by heat treatment at 320 °C for 5 h under argon atmosphere.

### 2.3. Characterization

The sulfur content in all the composites was determined with a CHNOS Elemental Analyzer (Vario Micro Cube, Elementar Americas). The morphology of the composites particles was evaluated by scanning electron microscopy (SEM, Leo FESEM). Atomic force microscopy (AFM, Agilent 4500 Series) imaging was detected under tapping mode. Zeta potential of graphene was determined using a laser electrophoresis zeta potential analyser (Zetasizer 3000HSA, Malvern Instruments). Powder X-ray diffraction (XRD, Bruker D8 Discover) analysis was carried out using Cu–Ka 1.1446 Å radiation at 40 kV. Fourier transformed infrared spectroscopy (FTIR, Bruker Vertex 70) analysis of KBr pellets were recorded in transmission mode. Thermogravimetric analysis (TGA, TA Instruments SDT Q600) was performed in nitrogen atmosphere at heating rate of 10 °C $min^{-1}$ to investigate the thermal stability of the composites.

The electrochemical performance of the composites was evaluated using lithium metal as counter and pseudo-reference electrode. The cathode was prepared by mixing active material, Katjen Black 600, and polyvinyldifluoride (PVDF) with a weight ratio of 8:1:1 using N-methylpyrrolidone (NMP) as solvent. The resulting slurry was painted onto nickel foam current collector (Φ12 mm) and dried at 60 °C for 12 h. The final electrode loading density was around 6–8 mg $cm^{-2}$ (total cathode material). CR2025 coin cells were assembled in an argon-filled glove box (Mbraun) using 1.0 M $LiPF_6$ in 1:1:1 v/v EC/DC/DMC as electrolyte and Celgard 2250 as separator. The cells were galvanostatically charge–discharged between 1 V and 3 V (*vs* $Li/Li^+$) using a battery tester (Neware Shenzhen, China). The specific capacities and rates reported here are based on the mass of sulfur. Cyclic voltammetry (CV) and electrochemical impedance spectroscopy (EIS) measurements were carried out on a Biologic VMP3 electrochemistry workstation. EIS was handled over the frequency range of 100 kHz–0.1 Hz and CV analysis was performed at scan rate of 0.1 mV $s^{-1}$.

## 3. Results and discussion

The preparation procedure of SAPN/RGO composite is illustrated in Fig. 1. Through the process, the exfoliated GO sheets in water are converted back to graphene by chemical reduction.

Zeta potential measurements confirmed the anionic charge of graphene sheets in water. The exfoliated GO shows a zeta potential of −55.7 mV, whilst that of hydrazine reduced RGO is −43.2 mV. This result implies that the carboxylic acid groups of GO are partially preserved when the reduction is conducted in the presence of ammonia. As a result, RGO can be dispersed due to the electrostatic forces.

RGO sheets cast on a silicon wafer were examined by AFM under tapping mode. Fig. 2 shows flat RGO sheets with a thickness of ~1 nm, implying the successful exfoliation from graphite to graphene sheets.

Fig. 3 depicts typical TGA curves of GO and RGO. The onset of mass loss for GO occurs at 200 °C, due to the pyrolysis of the labile oxygen containing functional groups leading to total decomposition of the material. The reaction is accompanied by an exothermic peak at 200 °C in the heat flow curve. Conversely, RGO shows about 65 wt.% residual mass after heating to 800 °C, and no obvious exothermic peak is detected in its heat flow curve. This is likely due to an increased thermal stability of the RGO after reduction of the oxygen functional groups and implies the successful formation of graphene.

The FTIR spectra of intermediates and composites materials are displayed in Fig. 4. After reduction of GO, the carboxylic and ketone

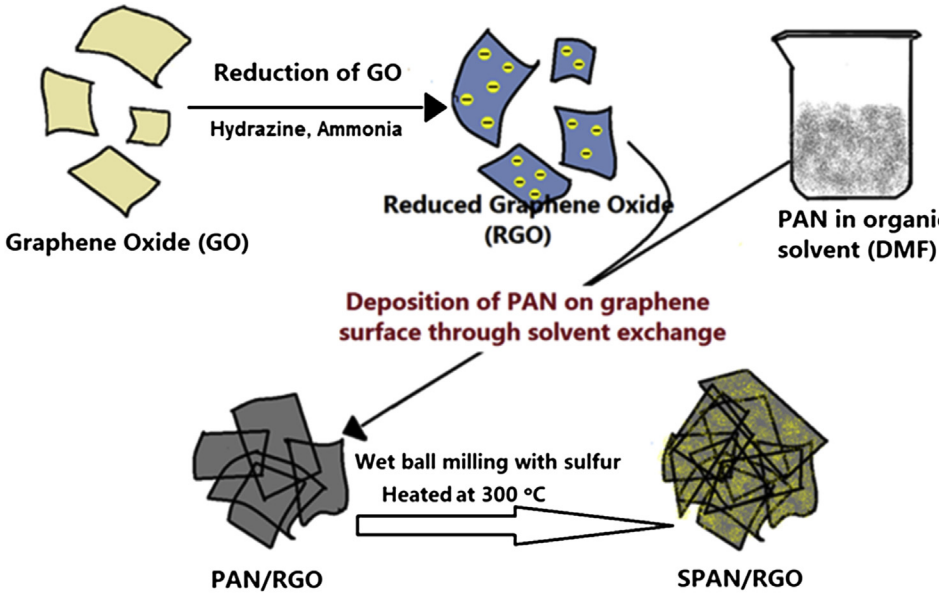


**Fig. 1.** Schematic of the solvent exchange process and synthesis of the SPAN/RGO composite.

C═O stretching vibration peaks at 1720 $cm^{-1}$ and 1630 $cm^{-1}$ are no longer observed in RGO pattern, confirming the successful reduction of GO by hydrazine with recovery of graphitic $sp^2$ configuration from $sp^3$ [32,33]. The appearance of the peak at 1570 $cm^{-1}$, typical of the carboxylate anion group, indicates partial preservation of polar groups from GO [31]. In the spectrum of PAN/RGO, the characteristic strong sharp peak at 2244 $cm^{-1}$ (relative to the cyano group stretching vibration) and the medium peak at 2940 $cm^{-1}$ confirm the presence of PAN in the composite. The additional peak located at 1571 $cm^{-1}$ attributes to the remaining carboxyl groups in RGO. Additionally, the peak at 1664 $cm^{-1}$ indicates that there might be interactions between PAN and RGO, such as electrostatic force between the cyano groups of PAN and the polar groups remained on RGO [9]. Furthermore, no apparent shift is observed for the peaks relative to the polyacrylonitrile functional groups, indicating that PAN is deposited but not covalently bonded to RGO (only electrostatic or long range interactions). On the contrary, the appearance of peaks in the 1000 $cm^{-1}$–1750 $cm^{-1}$ rang of the SPAN/RGO spectrum, corresponding to the pyrolyzed PAN backbone and the covalent bond between sulfur and carbon in the PAN matrix [34], implies successful reaction between sulfur and PAN.

The results of XRD measurements are presented in Fig. 5. The strong and narrow characteristic peak of graphite at 26.4° becomes broad in RGO pattern, and two new broad peaks emerge at 13.3° and 42.6°. This indicates an increase of interlayer spacing of pristine graphite, resulting from the addition of oxygen-containing functional groups after partial reduction of graphene oxide. [8] Besides the typical diffraction of PAN at 16.8° and 28.6°, a weak peak at 26.4° stemming from graphite is observed in the PAN/RGO pattern. However, the strong diffraction peak from RGO at 13.3° vanishes

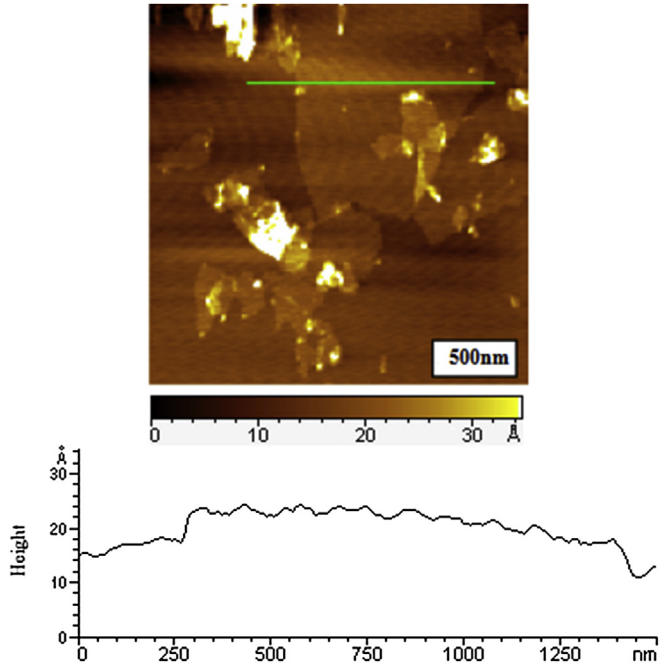


**Fig. 2.** AFM image of RGO sheets on a silicon wafer under tapping-mode with a cross-sectional height profile measured along the green straight line. (For interpretation of the references to colour in this figure legend, the reader is referred to the web version of this article.)

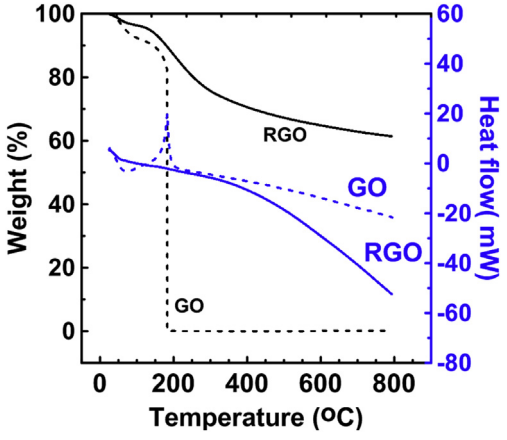


**Fig. 3.** TGA results of GO and RGO carried out under $N_2$ from room temperature to 800 °C.

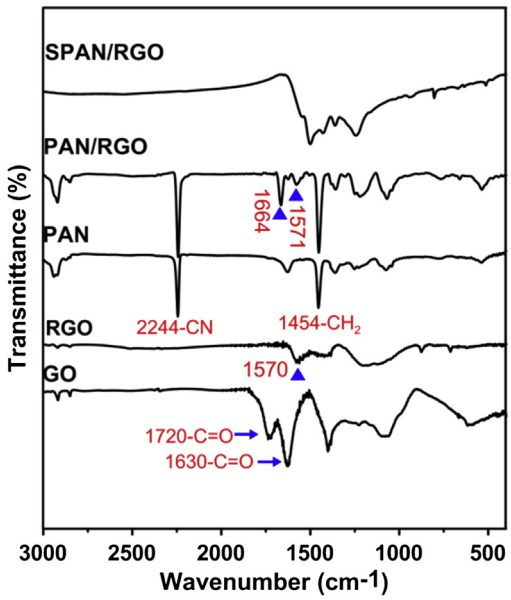


**Fig. 4.** FTIR spectra of GO, RGO, PAN, PAN/RGO, and SPAN/RGO.

due to the loss of graphitic layer order. In the SPAN/RGO composite with ~44 wt.% sulfur and ~3 wt.% RGO, a new broad peak at 24.9° appears but no typical characteristic diffraction from sulfur is observed, indicating the amorphous character of sulfur within the composite which seems to be uniformly dispersed in the PAN matrix. [7,36] The absence of characteristic peak of RGO in SPAN/RGO composite probably results from the low RGO content.

The SEM images of RGO, SPAN/RGO (44 wt.% S) and SPAN (46.2 wt.% S) composites are shown in Fig. 6. Strong agglomeration was observed in the dried RGO sheets (inset in Fig. 6A). The SPAN composite appears as a loose aggregation of small SPAN particles with average size of 200 nm (Fig. 6B). The morphology of the SPAN/RGO shows large aggregates with primary SPAN particles of much smaller size (around 100 nm) deposited on the surface of graphene (Fig. 6C). Hence, graphene cannot be identified in the SEM.

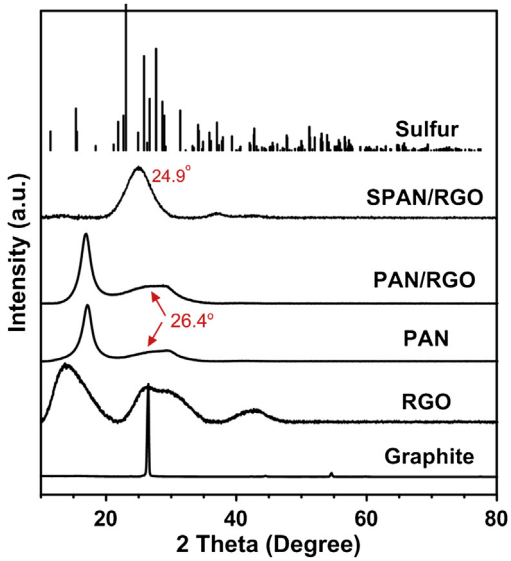


**Fig. 5.** XRD patterns of graphite, RGO, PAN, PAN/RGO, SPAN/RGO, and sulfur.

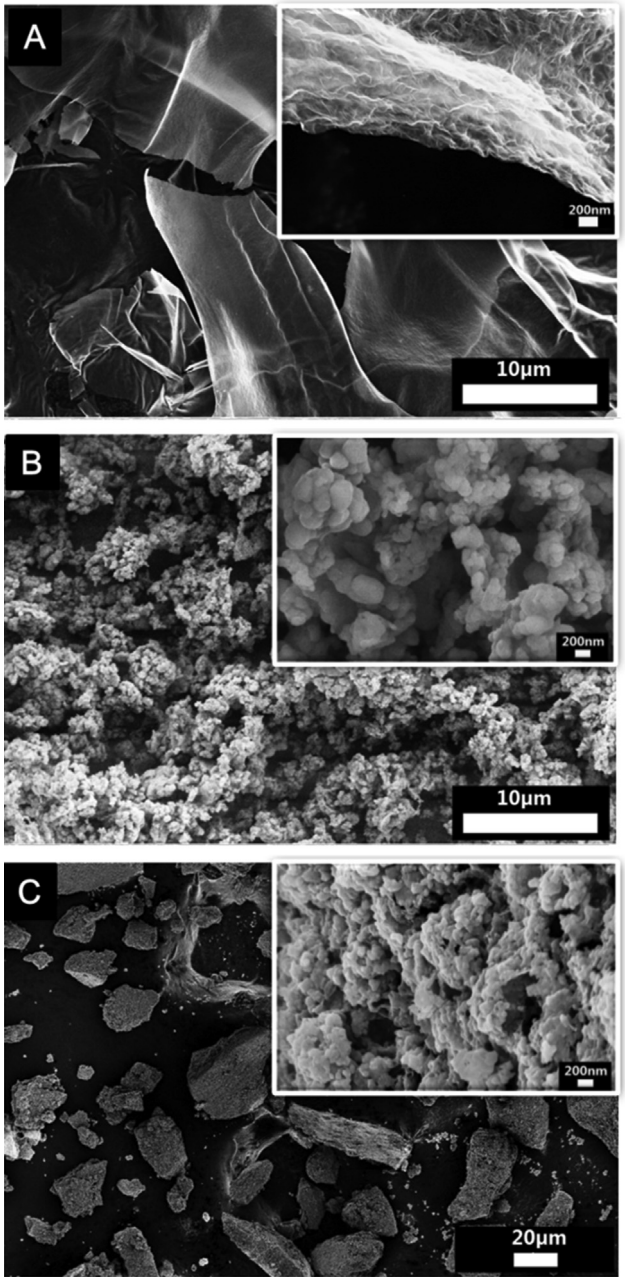


**Fig. 6.** SEM images of RGO (A), SPAN (B) and SPAN/RGO (C).

Galvanostatic discharge/charge curves of SPAN/RGO composite with 44 wt.% sulfur at 0.1C rate are depicted in Fig. 7. The initial discharge capacity of the composite is 1827 mAh $g^{-1}$, which is much higher than the theoretical capacity of sulfur (1675 mAh $g^{-1}$). The extra capacity is due to the irreversible insertion of lithium into the conjugated π-system of the PAN backbone [35]. In the second cycle, a reversible capacity of 1470 mAh $g^{-1}$ was achieved indicating 90% sulfur utilization. There is a very short potential plateau at ~2.35 V and a longer one at ~1.65 V in the first discharge curve. However, these two plateaus can hardly be distinguished in the 2nd and following cycles. Instead, only one potential plateau at about 1.8 V is portrayed. Additionally, the discharge/charge plateaus shift to higher values from the 1st to 10th cycle. Theoretically, there are two potential plateaus corresponding to the two-step reaction of sulfur with lithium at ~2.4 V and 2.1 V, respectively [36]. The lower potential for the second discharge plateau in the initial cycle is

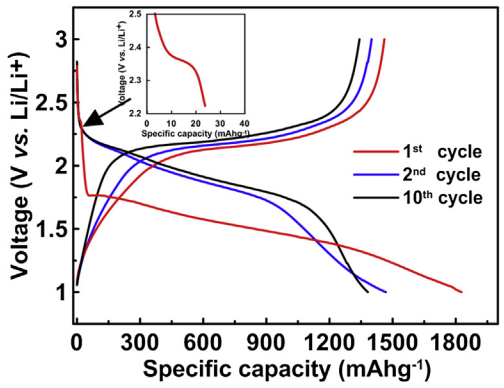


**Fig. 7.** Voltage *vs.* capacity profile of SPAN/RGO electrode (44 wt.% sulfur) at 0.1C rate between 1.0 and 3.0 V.

provoked by the additional energy needed to dissociate sulfur from the covalent bond with carbon in PAN backbone. Additionally, the highly dispersed elemental sulfur in short chain configurations inside the PAN matrix also contributes to the lower potential in the initial discharge due to their high energy state compared with large molecules of sulfur in crown ring structures [37,38]. The shorter potential plateau in the initial discharge (inset) indicates the existence of a very small amount of elemental sulfur which is not bound with PAN backbone. The shift in potential upon cycling is mainly due to the formation of the complexes with lower absorbing energy [38].

Fig. 8 shows the cyclic voltammograms of SPAN/RGO composite at a scanning rate of 0.1 mV $s^{-1}$. In the first cycle, it presents a weak cathodic peak at 2.35 V and a strong cathodic peak at 1.21 V, corresponding to the two-step reaction between lithium and sulfur. A strong anodic peak appears at 2.4 V, assigned to lithium ion extraction from $Li_2S_n$. In the subsequent cycles, the cathodic peak at 2.35 V disappears, while the cathodic peak at 1.21 V shifts positively, reaching 1.69 V in the 10th cycle. However, the anodic peak has only slight negative shift. These results are in good agreement with the charge–discharge curves.

The results of rate performance studies of the SPAN and SPAN/RGO composite electrodes are shown in Fig. 9. The discharge capacities of SPAN decrease steeply with increasing discharge rate, whereas the SPAN/RGO composite with ~3 wt.% graphene shows a much slower decline. The ternary composite delivers high capacities at relative high C-rates, namely, 1292 mAh $g^{-1}$ at 0.5C, 1180 mAh $g^{-1}$ at 1C, and 828 mAh $g^{-1}$ at 2C. Moreover, it shows good capacity recovery, with ~96% of the initial value attained at

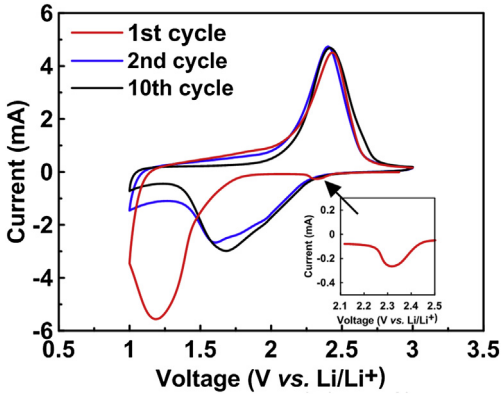


**Fig. 8.** Cyclic voltammograms of SPAN/RGO composite electrode at a scanning rate of 0.1 mV $s^{-1}$.

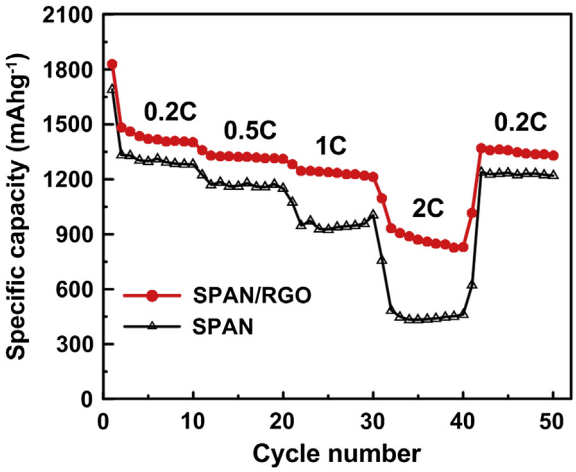


**Fig. 9.** Discharge capacity of SPAN and SPAN/RGO (3 wt.% RGO content) electrodes at different C-rates.

0.2C rate after high rate cycling, indicating that the composite has a very stable structure. Comparatively, the composite SPAN cathode without RGO delivers only half of the reversible capacity attained by the SPAN/RGO composite at 2C rate. This implies the SPAN/RGO composite has better conductivity confirming that the presence of highly conductive graphene sheets is instrumental to enhance the high rate performance in the sulfur–polymer cathode.

A close examination of the galvanostatic discharge and charge curves of SPAN and SPAN/RGO at different C-rates allows for the inspection of the effectiveness of RGO in reducing the potential polarization due to increased electrode resistance. As seen in Fig. 10a, the polarization of the SPAN/RGO composite electrode increases much more slowly than that of the SPAN composite upon increasing C-rate. This suggests that graphene significantly improves the electronic conductivity of the composite. EIS analysis of the SPAN/RGO and SPAN composites after the 10th discharge (Fig. 10b) corroborates the rate capability results. The SPAN/RGO composite has much lower charge transfer resistance, manifested by the smaller semi-circle at middle frequency.

The cycling performance of SPAN/RGO and SPAN at 0.1C rate is shown in Fig. 11. Both composites with and without RGO show similar capacity performance within the first 20 cycles. However, the SPAN composite cathode starts rapid capacity decay after 40 cycles, losing about 25% capacity by the 80th cycle. It eventually reaches 0 mAh $g^{-1}$ at the 100th cycle, which may be attributed to the dendrite growth due to the corrosion of the anode surface caused by the polysulfide shuttle [39]. Conversely, the SPAN/RGO composite with 3 wt.% RGO exhibits excellent cycle stability. After 100 cycles, the electrodes show overall 85% retention of the initial reversible capacity of 1467 mAh $g^{-1}$. Following the first discharge, the capacity rapidly decreases to 1385 mAh $g^{-1}$ in 10 cycles. Nevertheless, the SPAN/RGO composite delivers 1100 mAh $g^{-1}$ by the 200th cycle, which means 80% capacity retention within the last 190 cycles. Noteworthy, the Coulombic efficiency of the composite is close to 100% after 20 cycles, implying a very minute amount of shuttle effect.

The RGO sheets impart good conductivity and high surface area to the SPAN/RGO composite, providing a robust electron transport framework. In addition, the flexible graphene framework reinforces the structural stability of the electrode and enables the composite to accommodate the volume change of sulfur compounds during charge and discharge [25–28]. The functional groups on the RGO sheets might help prevent the dissolution of polysulfides from the electrode [9]. On the other hand, the presence of PAN in the

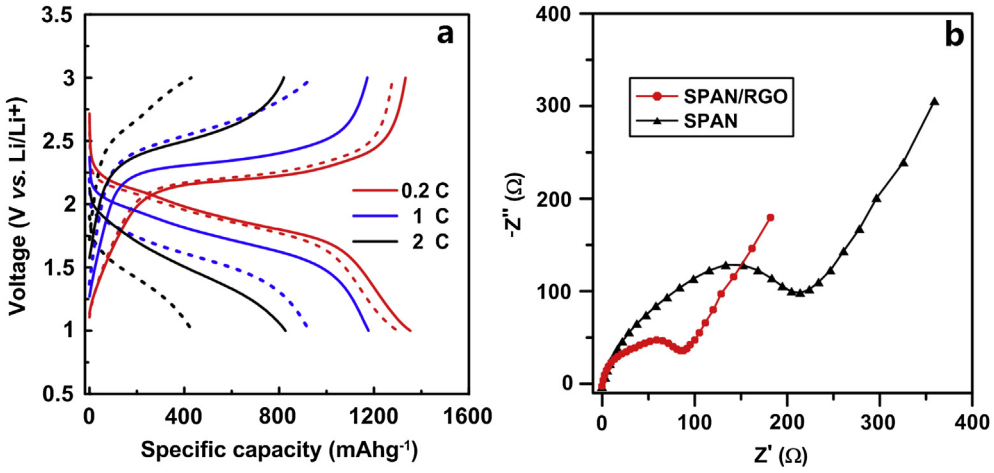


**Fig. 10.** (a) Fifth galvanostatic discharge/charge curves of SPAN (dashed line) and SPAN/RGO (solid line) at different C-rates and (b) EIS spectra of SPAN/RGO (44 wt.% S) and SPAN (46.2 wt.% S) after the 10th charge to 1.0 V at 0.1C rate, the inset is the enlarged image of SPAN/RGO spectra.

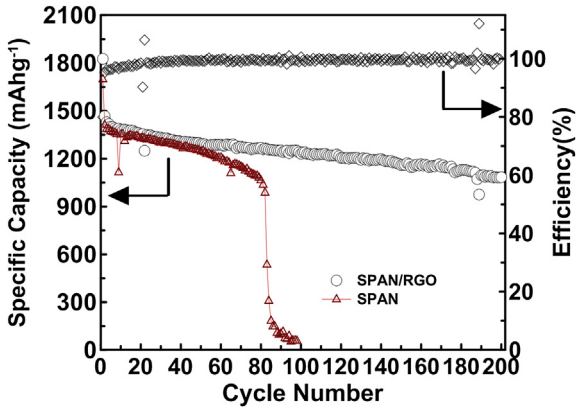


**Fig. 11.** Cycling performance of SPAN/RGO and SPAN composite electrodes at 0.1C rate.

composite helps maintain the polysulfides within the electrode. As a result, electrochemical polarization and the shuttle effect of polysulfides are suppressed, and the overall electrical performance of the sulfur cathode was significantly improved.

## 4. Conclusions

A sulfur–polyacrylonitrile/reduced graphene oxide composite was successfully synthesized. Graphene is shown to enhance the electrical conductivity and structural stability of the composite. The composite with 3 wt.% graphene retains ~80% of the stable reversible capacity (1385 mAh $g^{-1}$) over 200 cycles at a current density of 168 mA $g^{-1}$. The material exhibited good rate capability, and polarization at higher rates was significantly suppressed.

## References

[1] N. Jayaprakash, J. Shen, Surya S. Moganty, A. Corona, Angew. Chem. Int. Ed. 50 (2011) 5904–5908.
[2] J.A. Dean, McGraw Hill Book Co., New York, NY, 1985.
[3] Y. Cao, X. Li, I. a Aksay, J. Lemmon, Z. Nie, Z. Yang, J. Liu, Phys. Chem. Chem. Phys. 13 (2011) 7660–7665.
[4] X. Ji, L.F. Nazar, J. Mater. Chem. 20 (2010) 9821.
[5] G.-C. Li, G.-R. Li, S.-H. Ye, X.-P. Gao, Adv. Energy Mater. 2 (10) (October, 2012) 1238–1245.
[6] X. Liang, Z. Wen, Y. Liu, H. Zhang, J. Jin, M. Wu, X. Wu, J. Power Sources 206 (2012) 409–413.
[7] J. Wang, J. Yang, C. Wan, K. Du, J. Xie, N. Xu, Adv. Funct. Mater. 13 (2003) 487–492.
[8] L. Xiao, Y. Cao, J. Xiao, B. Schwenzer, M.H. Engelhard, L.V. Saraf, Z. Nie, G.J. Exarhos, J. Liu, Adv. Mater. (Deerfield Beach, Fla.) 24 (2012) 1176–1181.
[9] L. Yin, J. Wang, F. Lin, J. Yang, Y. Nuli, Energy Environ. Sci. 5 (2012) 6966.
[10] X. Ji, K.T. Lee, L.F. Nazar, Nat. Mater. 8 (2009) 500–506.
[11] G. He, X. Ji, L. Nazar, Energy Environ. Sci. 4 (2011) 2878.
[12] Y.-S. Su, A. Manthiram, Electrochim. Acta 77 (2012) 272–278.
[13] X. Li, Y. Cao, W. Qi, L.V. Saraf, J. Xiao, Z. Nie, J. Mietek, J.-G. Zhang, B. Schwenzer, J. Liu, J. Mater. Chem. 21 (2011) 16603.
[14] J. Kim, D.-J. Lee, H.-G. Jung, Y.-K. Sun, J. Hassoun, B. Scrosati, Adv. Funct. Mater. 23 (8) (February 25, 2013) 1076–1080.
[15] X. Liang, Z. Wen, Y. Liu, H. Zhang, L. Huang, J. Jin, J. Power Sources 196 (2011) 3655–3658.
[16] S. Wei, H. Zhang, Y. Huang, W. Wang, Y. Xia, Z. Yu, Energy Environ. Sci. 4 (2011) 736.
[17] C. Zhang, H. Bin Wu, C. Yuan, Z. Guo, X.W.D. Lou, Angew. Chem. Int. Ed. 124 (38) (September 17, 2012) 9730–9733.
[18] G. Zheng, Y. Yang, J.J. Cha, S.S. Hong, Y. Cui, Nano Lett. 11 (2011) 4462–4467.
[19] R. Elazari, G. Salitra, A. Garsuch, A. Panchenko, D. Aurbach, Adv. Mater. (Deerfield Beach, Fla.) 23 (2011) 5641–5644.
[20] J. Guo, Y. Xu, C. Wang, Nano Lett. 11 (2011) 4288–4294.
[21] L. Ji, M. Rao, S. Aloni, L. Wang, E.J. Cairns, Y. Zhang, Energy Environ. Sci. 4 (2011) 5053.
[22] L. Yin, J. Wang, J. Yang, Y. Nuli, J. Mater. Chem. 21 (2011) 6807.
[23] W. Wei, J. Wang, L. Zhou, J. Yang, B. Schumann, Y. NuLi, Electrochem. Commun. 13 (2011) 399–402.
[24] H. Wang, Y. Yang, Y. Liang, J.T. Robinson, Y. Li, A. Jackson, Y. Cui, H. Dai, Nano Lett. 11 (2011) 2644–2647.
[25] Y.-X. Wang, L. Huang, L.-C. Sun, S.-Y. Xie, G.-L. Xu, S.-R. Chen, Y.-F. Xu, J.-T. Li, S.-L. Chou, S.-X. Dou, S.-G. Sun, J. Mater. Chem. 22 (2012) 4744.
[26] L.S. Cells, L. Ji, M. Rao, H. Zheng, L. Zhang, O.Y. Li, W. Duan, JACS (2011) 18522–18525.
[27] J.-Z. Wang, L. Lu, M. Choucair, J. a. Stride, X. Xu, H.-K. Liu, J. Power Sources 196 (2011) 7030–7034.
[28] F. Zhang, X. Zhang, Y. Dong, L. Wang, J. Mater. Chem. 22 (2012) 11452.
[29] M. Sen Zheng, Z.K. Wei, Q.F. Dong, Adv. Mater. Res. 460 (2012) 74–77.
[30] R.E.O. William, S. Hummers Jr. 208 (1957) 1937.
[31] D. Li, M.B. Müller, S. Gilje, R.B. Kaner, G.G. Wallace, Nat. Nanotechnol. 3 (2008) 101–105.
[32] S.A. Ju, K. Kim, J.-H. Kim, S.-S. Lee, ACS Appl. Mater. Interfaces 3 (2011) 2904–2911.
[33] J. Zhang, H. Yang, G. Shen, P. Cheng, J. Zhang, S. Guo, Chem. Commun. (Cambridge, England) 46 (2010) 1112–1114.
[34] J. Fanous, M. Wegner, J. Grimminger, Ä. Andresen, M.R. Buchmeiser, Chem. Mater. 23 (2011) 5024–5028.
[35] A.G. Macdiarmid, Angew. Chem. Int. Ed. (2001) 2581–2590.
[36] Y.V. Mikhaylik, J.R. Akridge, J. Electrochem. Soc. 151 (2004) A1969.
[37] V.V Shinkarev, V.B. Fenelonov, G.G. Kuvshinov 41 (2003) 295–302.
[38] B. Zhang, X. Qin, G.R. Li, X.P. Gao, Energy Environ. Sci. 3 (2010) 1531.
[39] V.S. Kolosnitsyn, E.V. Karaseva, Russ. J. Electrochem. 44 (2008) 506–509.